IEEE Robotics and Automation Letters (RAL) paper presented at the
2020 IEEE/RSJ International Conference on Intelligent Robots and Systems (IROS)
October 25-29, 2020, Las Vegas, NV, USA (Virtual)

LineSpyX: A Power Line Inspection Robot Based on Digital Radiography

Yuan Gao, Guangming Song, *Senior Member*, *IEEE*, Songtao Li, Fushuai Zhen, Dabing Chen, and Aiguo Song, *Senior Member*, *IEEE*

***Abstract*—Most of the current power line inspection robots use cameras and LiDARs to inspect the power line surfaces and the surrounding environment. But it is still difficult to detect the internal defects of the power lines. In this paper, the design and implementation of LineSpyX, a novel power line inspection robot based on digital radiography (DR), is introduced to solve the problem of non-destructive testing (NDT) of the overhead Aluminum Conductor Composite Core (ACCC) wires. The proposed robot has a stable wrapped mechanical structure with a moving system, a live work system, and a NDT system. The wheeled moving system enables the robot to move on the wires and cross obstacles such as vibration dampers. The NDT system consists of a portable X-ray generator and a DR detection panel. When the robot performs the inspection task, the X-ray goes up through the ACCC wire to the panel, where the X-ray images of the internal carbon fiber cores are recorded. A deep learning based defect diagnosis method combined with manual diagnosis is proposed to detect potential defects. The main functionalities of the developed robot are verified by lab experiments and field tests.**

I. Introduction

The Aluminum Conductor Composite Core (ACCC) wire, as a new type of conductor with light weight and high conductivity, has been widely used in power grid globally. But the composite core in the ACCC wire is easy to be damaged in non-standard construction processes. And wire breakage accidents will occur when the composite cores are damaged by long-time tension and vibration. Starting from this decade, ACCC wire breakage accidents did occasionally occur worldwide and caused massive losses. Therefore, an efficient inspection method for overhead ACCC wires is urgently needed to ensure the safety of power grid.

Traditionally, most of the inspection tasks of power lines are done by human, which is ineffective, high-cost and dangerous. Recently, with the development of robotics and automation, the power inspection robot replaces manual inspection gradually and becomes an important part of inspection tools to maintain the power grid system [1]. After years of development, the technologies of power line inspection robots have become relatively mature with multiple functions available such as inspection [2-11], maintenance [12-14], and non-destructive testing (NDT) [15-19]. Most of the current power line inspection robots use cameras and LiDARs to inspect the power line surfaces, or use special tools to perform the maintenance task. Because of the limitation of the weight, size and power of NDT devices, the inspection robots that can detect the defects inside the overhead transmission lines are scarce.

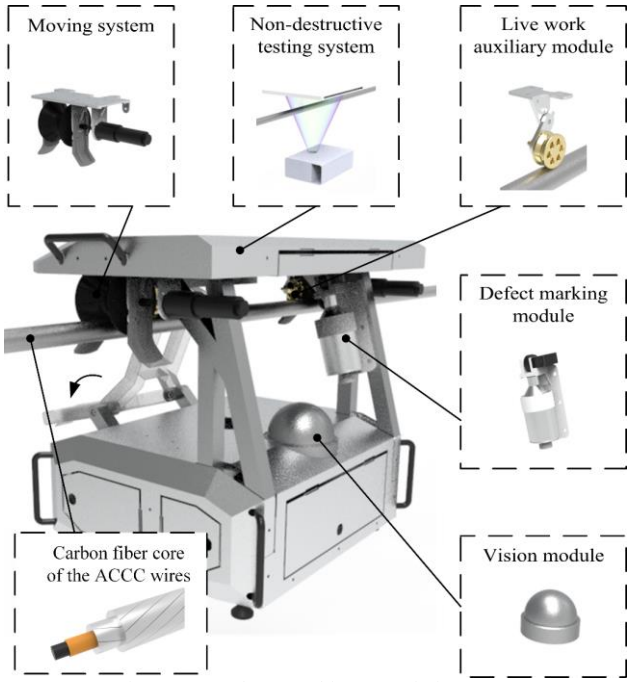

Figure 1. Hardware architecture of LineSpyX.

Several NDT technologies for the overhead transmission lines have been developed recently. Depending on the different deployment methods, the existing NDT technologies mentioned above can be divided into two categories. One is that the sensors are fixed on wires, such as ultrasonic guided wave (UGW) [20], power line carrier (PLC) [21], etc. The principles of UGW and PLC are almost the same, that they detect the reflected signal generated by the defect at the same time of transmitting the signal. The shortcoming of UGW and PLC is that these methods are easily affected by noise or reflections from the discontinuities in transmission lines, which will cover the reflected signal of defect completely and cause misdiagnosis. The other is that the sensors are embedded on robot, such as infrared ray, electromagnetic, magnetic flux leakage (MFL), eddy current, and X-ray et al. Many power line inspection robots are equipped with infrared ray devices to detect abnormal temperatures at the lines with

*Research supported by the National Natural Science Foundation of China under Grant 61973076 and in part by Science and Technology Project of State Grid Corporation of China under Grant 5200-201918120A-0-0-00.

Y. Gao, G. Song, S. Li, F. Zhen and A. Song are with the State Key Laboratory of Bioelectronics, Jiangsu Key Lab of Remote Measurement and Control, School of Instrument Science and Engineering, Southeast University, Nanjing, 210096 China. (corresponding author :Guangming Song, phone: 86-025-83793293, email: mikesong@seu.edu.cn;).

D. Chen is with the State Grid Jiangsu Electric Power Co., Ltd Research Institute, Nanjing, 211103 China.

potential defects. However, the infrared ray NDT device is susceptible to environmental effects such as sunlight which may cause the false detection. Pinto et al. [15] from Eletrobras-Cepel, Brazil designed an inspection robot based on electromagnetic to detect the internal defects in Aluminum Conductors Steel Reinforced (ACSR) wires. Jiang et al. [16] from Chongqing University, China designed an inspection robot based on MFL, which equipped a sensor with heavy permanent magnets and Hall elements to detect the breakage of the steel core in ACSR wires. Pouliot et al. [17] from IREQ, Canada proposed a sensor prototype based on MFL and a sensor based on eddy current named LineCore. The LineCore sensor has the capability to perform the inspection of the zinc layer erosion on the steel core in ACSR wires. It can be embedded on power line inspection robots such as LineScout. Furthermore, Mirallès et al. [18] from IREQ, Canada designed the LineDrone, which innovatively uses the fly-glide structure of UAV and carries the LineCore sensor to realize the NDT of ACSR wires. However, due to the lack of eddy current characteristics in the carbon fiber core of the ACCC wires, the devices above cannot complete the non-destructive inspection of the ACCC wires. Though the idea of adding magnetic cover to the composite core in the ACCC wire is mentioned in paper [22], it is still helpless to solve the problem of NDT of the ACCC wires running in the grid. To the best of our knowledge, currently there are few power line inspection robots that can perform NDT of overhead ACCC wires.

The X-ray NDT devices become portable with the development of digital radiography (DR), so the DR system has been applied in power line detection tentatively. Pouliot et al. [17] from IREQ, Canada proposed a prototype based on X-ray, to detect the wire splinter defects of overhead ACSR wires inside the suspension clamps. Tsukuba Technology Co., Ltd, Japan [19] designed a portable X-ray inspection device with the function of NDT for internal defects of ACSR wires. The devices above have verified the feasibility of power line NDT based on DR, but with shortcomings in the capabilities of moving and obstacle crossing. Among the NDT technologies mentioned above, the DR system is currently the best choice for the NDT of overhead ACCC wires.

In this paper, the design and implementation of LineSpyX, a novel inspection robot for NDT of overhead ACCC wires, is introduced. The proposed robot is in the form of a wrapped structure for mechanical stability, and is powerful to cross obstacles like vibration dampers. LineSpyX can get the X-ray images of the carbon fiber cores by integrating a NDT system based on DR. Furthermore, a deep learning based defect diagnosis method combined with manual diagnosis is proposed to detect carbon fiber core defects. The main contributions of this paper are threefold. First, the design method of a novel power line inspection robot architecture is of great value in engineering. The proposed method will greatly alleviate the technology and equipment shortage in the NDT of overhead ACCC wires, which is now an urgent problem in the power line inspection and maintenance industry. Second, the combination of DR and robotics makes the NDT efficient and flexible, and the proposed technology can be migrated to other industries. Lastly, the defect diagnosis method based on deep learning improves the work efficiency and is stable in the industrial environment.

II. System Platform Design

A Design overview

According to a report from State Grid, China, the causes of ACCC wire breakage accidents are divided into two categories. One is the tensile failure in strain clamps, the other is the bending break caused by non-standard tools during the construction. The locations of breakage accidents are all within 15m from each end of the transmission line. So the working space of LineSpyX is set to each end of the transmission line within 30m, which covers the failure-prone area mentioned above. Besides, the overhead transmission lines are most in the multi-bundled form. LineSpyX can operate on the multi-bundled conductors and perform the NDT task one sub-conductor at a time. So LineSpyX should be convenient to be installed, to switch among sub-conductors quickly with the help of a single lineman. Further, the capability of climbing and obstacle crossing is also important to LineSpyX. Therefore, it can adapt to overhead transmission lines with altitude differences and to cross obstacles such as clamps and vibration dampers. Lastly, the NDT system of LineSpyX should have good performance in imaging quality, efficiency and stability.

LineSpyX is composed of the hardware platform and the control system. The hardware platform consists of the wrapped body, the moving system, the NDT system and a variety of functional components. The 3d model of LineSpyX is shown in Fig. 1. The robot body is in a form of wrapped structure, with a baffle that can be locked on one side to facilitate installation and ensure the overall structure stability. The moving system consists of two sets of rubber wheels driven by decelerating motors, which are distributed along the

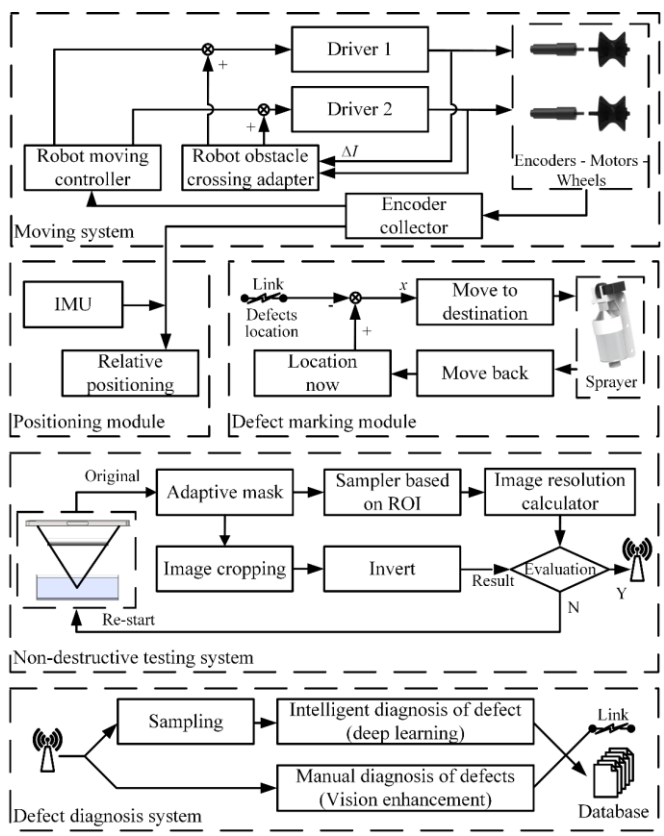

Figure 2. Architecture of the overall control system.

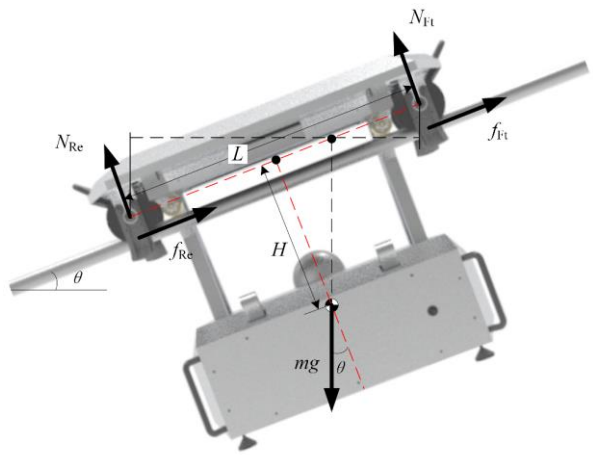

Figure 3. Force analysis of the proposed robot when it is climbing.

direction of detection. The NDT system consists of a portable X-ray generator and a DR detection panel, and the ray from the X-ray generator goes up through the ACCC wire to the panel. Among the functional modules, the live work auxiliary module is made up of a stretchable non-power copper wheel, which is used to contact the wire to keep the robot equipotential and is a key module to expand the application of LineSpyX in live work. The defect marking module is an automatic spray paint controlled by defect diagnosis system for marking the defect location on ACCC wires, which facilitates reinforcement and maintenance later. The vision module is a pan-tilt camera for remote operation.

The control system is composed of five parts. As shown in Fig. 2, the moving system, the NDT system, the defect diagnosis system, the positioning module and the defect marking module are scheduled by the controller to realize main functions of the robot.

B Moving system

The moving system of LineSpyX is composed of two independent rubber wheels, and the driving force is provided by the dc motors with reducers. The normal moving speed is 6m/min.

The forces acting on the robot when it is climbing the transmission line are shown in Fig. 3. Taking the robot body as the research object, the supporting forces of the front and rear wheels are N_{Ft} and N_{Re}, and the direction is perpendicular to the wire. The friction forces on the front and rear wheels are f_{Ft} and f_{Re}, which are static friction forces assuming no slip. The distance between the two wheels is L, and the vertical distance between the center of gravity and the wheel is H. From the force relation, it is easy to get:

$$\begin{aligned} N_{Ft} &= (\frac{1}{2}\cos\theta + \frac{H}{L}\sin\theta)mg \\ N_{Re} &= (\frac{1}{2}\cos\theta - \frac{H}{L}\sin\theta)mg \end{aligned} . \quad (1)$$

Apparently, the supporting force of the front wheel is greater than that of the rear wheel. Furthermore, the maximum static friction f_{max} is related to the supporting force N:

$$f_{Ft\,max} > f_{Re\,max} . \quad (2)$$

The friction of the front wheels of the robot is larger, so the rear wheel is easier to slip under the same driving force. In extreme cases, the rear wheel will vacate, so the maximum climbing angle of the robot is shown in (3):

$$\theta_{max} = \min\left\{\arctan\left(\frac{L}{2H}\right), \arcsin\left(\frac{f_{Fr}+f_{Re}}{mg}\right)\right\}. \quad (3)$$

Furthermore, applying the analysis above to the obstacle crossing process, if the front wheel can cross the obstacle, the rear one will cross that easily.

In the motion simulation tests, when the angle of the wire is 20 degrees, the speed and force of the robot are shown in Fig. 4. When both the two wheels are on the wire, the robot moves at a constant speed. When the front wheel is located on the performed armor rod, the torque of the front wheel increases while that of the rear wheel decreases to a negative number due to the difference in the actual radius of the front and rear wheels. The wheel diameter mismatch mentioned above causes the robot speed fluctuation. When crossing the vibration damper, the torques of both wheels increase and the time is shorter. After the obstacle crossing, the two wheels are

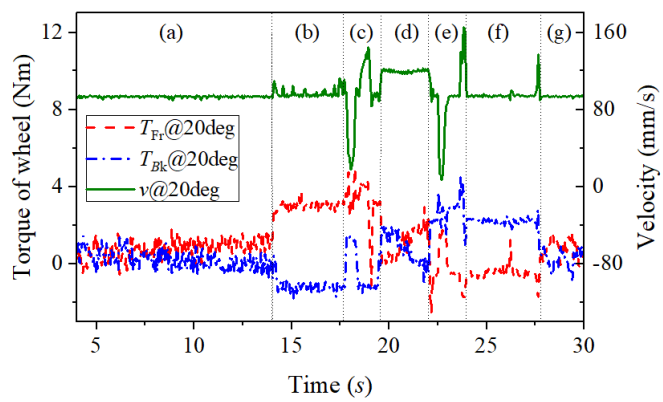

Figure 4. Torque of wheels and velocity of robot when it crosses the obstacle with a climbing angle of 20 degrees.

(Notes: Part a & g: LineSpyX is climbing the line only. Part b& f: LineSpyX's front/rear wheel is climbing the performed armor rod, speeds of the front and rear wheels are not match. Part c & e: LineSpyX is climbing the vibration damper. Part d: Both wheels of LineSpyX are on the performed armor rod, speed is faster than normal.)

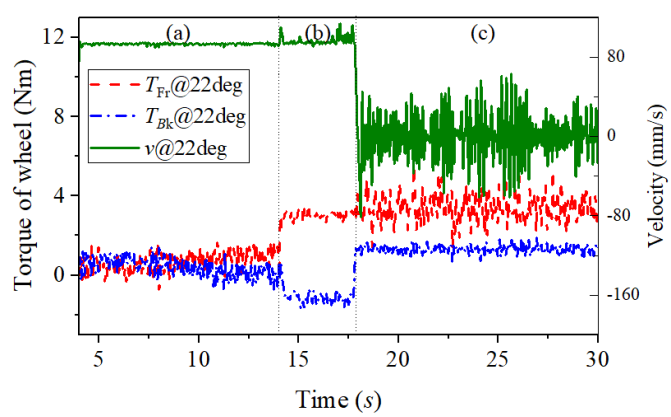

Figure 5. Torque of wheels and velocity of robot when it fails to cross the obstacle with a climbing angle of 22 degrees.

(Notes: Part a: LineSpyX is climbing the line only. Part b: LineSpyX's front/rear wheel is climbing the performed armor rod, speeds of the front and rear wheels are not match. Part c: LineSpyX is stuck by vibration damper, obstacle crossing task is failed.)

both located on the performed armor rod, and the speed of the robot is increased. Similarly, then the rear wheel moves over the vibration damper. Summing up the above, in the process of completing the obstacle crossing task, the conflict of the motor output occurs, caused by the mismatch of the linear speed between the two wheels. In the contrast experiment, the angle of wire is set to 22 degrees, and the parameters of the robot motion are shown in Fig. 5. When the robot tries to cross the obstacle by the front wheel, it fails, and the speed drops to zero. In general, if the motor output conflict caused by the velocity mismatch between the front and rear wheels is solved, the speed of the robot before climbing the slope will be effectively improved. The kinetic energy of the robot during obstacle crossing will also be improved, so that the obstacle crossing capability will be improved. Therefore, a speed controller is designed for the obstacle crossing process.

The moving system controlled by a controller for normal state and an adapter for obstacle crossing. As shown in Fig. 2, the current sensor is attached to the wire of motor, which reflects the motor output power. When the current difference between the front and rear wheel exceeds the threshold, the velocity of the lower power output wheel will be increased slightly. The adapter is based on a PD controller which is given by:

$$v' = v + K_p \Delta I + K_d (\Delta I - \Delta I'), \tag{4}$$

where ΔI is the current difference, K_p and K_d is the parameters of PD controller, v is the velocity.

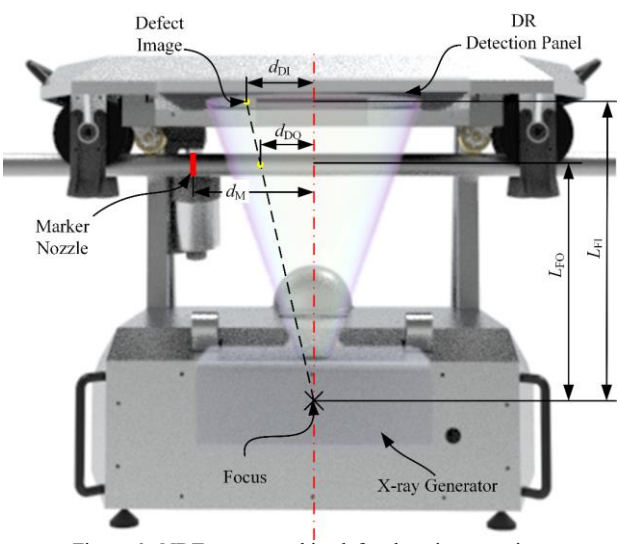

Figure 6. NDT system and its defect location mapping.

TABLE I. PARAMETERS OF THE NDT SYSTEM

Parameters	Values
Focus diameter of X-ray generator	0.5mm
Ray angle of X-ray generator	40°
Power of X-ray generator *	80kV@0.6mA
Pixel size of DR detection panel	2508×3004
Resolution of DR detection panel	5lp/mm
Settling time of DR detection panel *	1.5s
Distance between focus and object, L_{FO}	176mm
Distance between focus and image, L_{FI}	247mm

*Appropriate parameters for the 450/55 ACCC wires

C NDT system

The NDT system based on DR consists of a portable X-ray generator and a DR detection panel, which are installed at the bottom and the top of the robot respectively in parallel. As shown in Fig.6, for stability and safety reasons, the X-ray generator is installed at the bottom of the robot, and the installation position ensures that the robot does not interfere with the vibration damper in the obstacle crossing task. The key parameters of the NDT system are listed in Table I. Some parameters are slightly different when LineSpyX is operating on different ACCC wires, whose diameters range from 15.3mm to 35mm. In this paper, the detection object is the 450/55 ACCC wire with two layers of enveloped aluminum wires, and its diameter is 26.4mm.

$$T_X = \frac{L_{FI}}{L_{FO}}, \tag{5}$$

where L_{FO} is the distance between focus and object, L_{FI} is the distance between focus and image. Referring to the parameters in Table I, the magnification of DR system T_X is 1.4. In addition, there is a shadow at the edge, caused by scattered rays. So the marginal area should be omitted during the detection.

In order to prevent the blind area of detection, LineSpyX reserves coincidence area. At this point, the features in the image can fully reflect the internal characteristics of the ACCC wires. The position can be mapped by:

$$d_{DO} = \frac{d_{DI}}{T_X}, \tag{6}$$

where d_{DO} and d_{DI} are based on the center line of the robot, and positive represents the forward direction.

The defect marking system of the robot is used to mark the defect positions detected by the diagnostic system, to facilitate the defect location during maintenance service. Because the defect diagnosis at the user terminal consumes a large amount of time, the defect cannot be marked in real time. When the robot receives the defect position from the user terminal, the marking task is created immediately. After the completion of the detection task, the robot will move to the destination, and paint on the wire. The range of paint is shown in:

$$\begin{cases} \mathbf{M} = \left[X - \frac{L_M}{2}, X + L_M + \frac{L_M}{2} \right], \\ X = x_i - x_{i-k} + d_M - \frac{d_{DI}}{T_X} \end{cases} \tag{7}$$

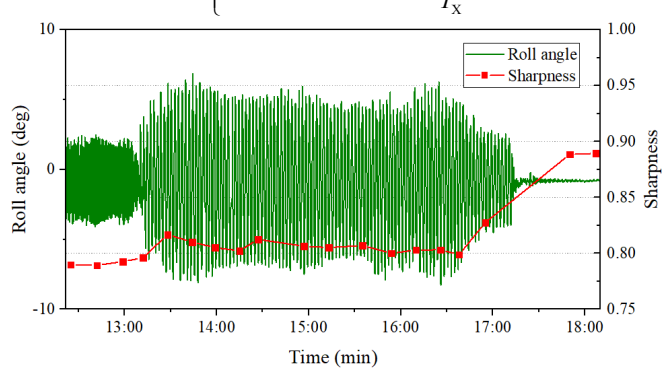

Figure 7. Relationship between robot vibration and DR imaging clarity.

where i is the natural number index. k is the interval period, no more than 2. The robot receives the marking signal at t_i, and the position of robot is x_{i-k} at t_{i-k} when the robot detected the defect. L_M is the length of mark, and the defect is in the mark center theoretically.

After the marking task, the robot moves back to the position where it is interrupted, and the inspection task will go on. The relative positioning module, combined with the encoders and IMU, provides an important service here.

D *Imaging clarity evaluation*

Because the settling time is required when the digital radiography detection panel is working, the more stable the robot is, the better imaging quality the panel will have. Because the robot runs on a single wire and is a typical underactuated system in the roll direction, it is susceptible to shaking under the influence of wind load and wire vibration. So the un-sharpness caused by motion is the biggest factor that affects the imaging quality. As shown in Fig. 7, compared with multiple images collected at the same position, the sharpness is worse when shaking.

The criterion of imaging resolution in LineSpyX is Laplacian gradient as shown in (8), which is isotropous [23-24]. In the image collected by the NDT system, the texture is inclined. The gradient function of Laplacian operator is sensitive to texture edges in all directions, so it can reflect the resolution of the detection image. Furthermore, the gradient value is normalized and 0.8 is set as the threshold value which can effectively distinguish the valid image from invalid one.

$$\boldsymbol{D}\left(\boldsymbol{I}_{\text{img}}\right)=\sum\left|\frac{1}{6}\begin{bmatrix}1 & 4 & 1\\ 4 & -20 & 4\\ 1 & 4 & 1\end{bmatrix}\otimes\boldsymbol{I}_{\text{img}}\right|. \tag{8}$$

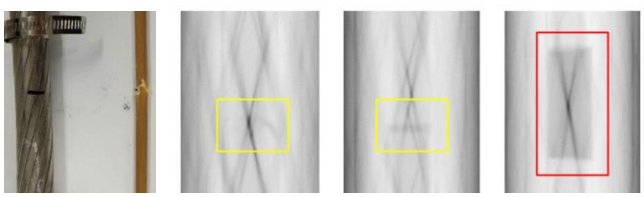

(a) (b) (c) (d)

Figure 8. Typical defect samples of ACCC wires.
(a) An ACCC core sample with a defect. (b) An inverted X-ray image of a sample with slight cracks. (c) An inverted X-ray image of a sample with breakage. (d) An inverted X-ray image of a sample with a pulled-apart defect.

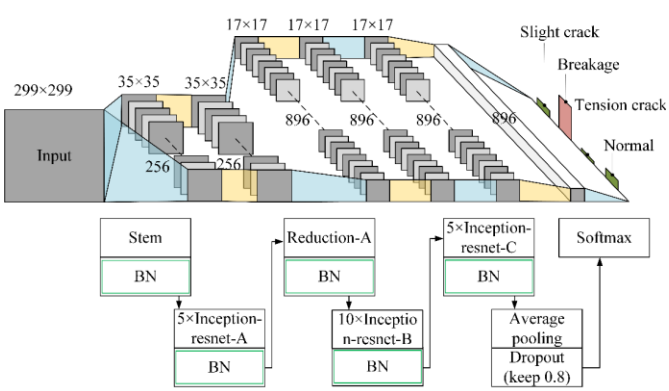

Figure 9. The CNN architecture in the intelligent defect diagnosis module.

III. Defect Diagnosis

In this defect diagnosis system, the Convolutional Neural Network (CNN) is used as the intelligent defect diagnosis module, and the manual defect diagnosis module based on the vision-enhanced method is used as an assistant to determine and locate the defects of the carbon fiber core in ACCC wires.

The typical defects of ACCC wires are shown in Fig. 8. Fig. 8b is slight damage, showing cracks with irregular lines, which are of medium risk. Fig. 8c is breakage, which is characterized by the break of carbon fiber core and the stressed part is the outer aluminum wire. This condition is dangerous. Fig. 8d is tension crack, which is manifested as the vacancy caused by carbon fiber core pulled apart after break. This condition is extremely dangerous.

The intelligent defect diagnosis module uses a multi-class neural network based on the modified Inception-resnet-V2 network [25], which is shown in Fig. 9. In the classifier, the sample without defect is negative, and the positive samples are divided into slight crack, breakage and tension crack. In order to improve the convergence speed and increase the accuracy, the Reduction-B layer is deleted and the BN layers are added.

Before training, a large amount of samples are collected in the laboratory, and Generative Adversarial Networks (GAN) is used to extend the samples. So that, there are 64410 samples available, with 30500 positive samples included. The training set and verification set are allocated from the samples in proportion of 5:4. One frame of sample should be cut into small pieces according to the fixed size, to improve the perception field, so as to improve the effect of recognition.

The verification results are shown in Table II, the recognition rate of positive samples is 89.67%, and that of negative samples is 99.7%. The causes of misdiagnosis can be summarized as the unobvious defects in positive samples and the suspected defects in negative samples.

As an assistant, the manual defect diagnosis can prevent

TABLE II. Verification Results

	Positive samples (with defect)	**Negative samples (without defect)**
Total verfication set	12628	12301
Misdiagnosis set	1305	36
Recognition rate	89.67%	99.70%

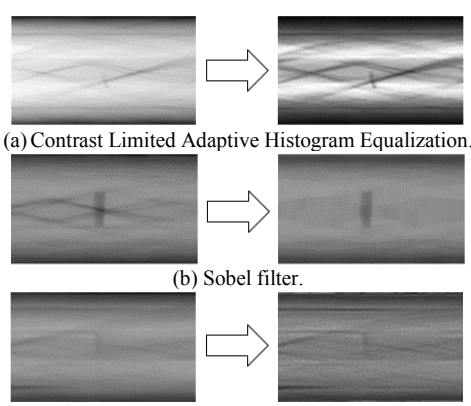

(a) Contrast Limited Adaptive Histogram Equalization.
(b) Sobel filter.
(c) Un-shap masking.

Figure 10. Vision enhancements for manual defect diagnosis.

misdiagnosis effectively. However, the interference of the outer enveloped-aluminum shadow in the collected image is not conducive to manual diagnosis. In this module, Contrast Limited Adaptive Histogram Equalization (CLAHE), Sobel filter, and un-sharp masking methods are used to improve the identification of defects. As shown in Fig. 10, the CLAHE method increases the gray value of specific image elements, but without adding noise. The Sobel filter method can extract the texture in specific direction, which is helpful to separate the defect feature from the enveloped aluminum shadow. The un-sharp masking method reduces the clear edges and magnifies the unclear edges, which is helpful for the appearance of unclear defect features. All the images processed by the methods above display on the user terminal side by side for the sake of diagnosis. After that, the results of intelligent and manual defect diagnosis are stored in the database for later review.

IV. Experiments

A Prototype and Lab Experiments

The prototype of LineSpyX is 60 cm long, 41 cm wide and 50 cm high, the weight is 25kg, and the moving speed is 6 m/min at normal. The power system is designed with dual power supply, where, the NDT system is powered by 24v10Ah battery alone, which can ensure the operation for 70 minutes. The central controller is ARK1123, with Linux and OpenCV, which can meet the requirement of robot control and image preprocessing. The user terminal is an industrial computer with TensorFlow, which is easy-used and sufficient for defect diagnosis.

The Lab experiments are conducted to test the motion performance and system stability. As shown in Fig. 11, the testbed is a 22m long ACCC wire, with adjustable sag. The results in Table III show that the maximum climbing angle is 35 degrees when climbing the wire without obstacles, and the maximum climbing angle decreases to 25 degrees when climbing the wire with a vibration damper.

Figure 11. Testbed of Lab experiments.

TABLE III. Field Test Results

Angle	Climbing with no obstacle	Climbing with Vibration damper
10°	✓	✓
15°	✓	✓
20°	✓	✓
25°	✓	○
30°	✓	×
35°	✓	×
40°	×	×

Note: "✓": LineSpyX can complete the task.
"○": LineSpyX fails sometimes.
"×": LineSpyX cannot run under this circumstance.

Figure 12. Field tests in Suzhou, China, in October 2019.

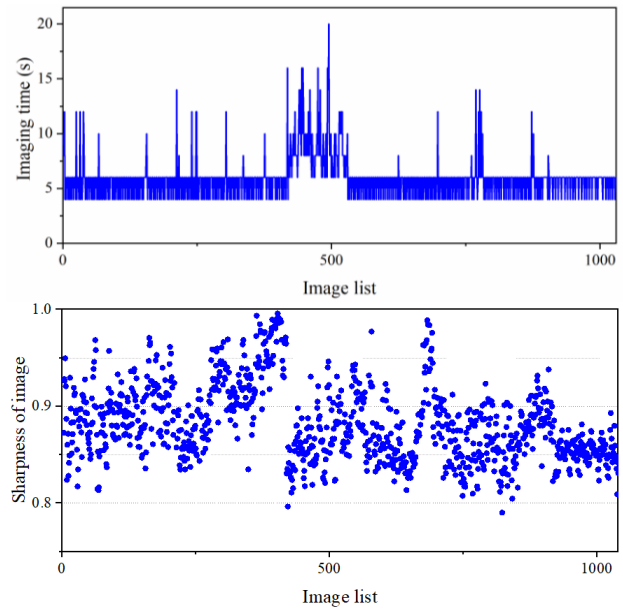

Figure 13 (a). The imaging times of the X-ray images.
(b). Image resolution in the field test, the qualification rate is 99.8%.

B Field Tests

LineSpyX has been tested in several field tests. In October, 2019, as shown in Fig. 12, an application test on a newly-built transmission line in Suzhou, China was completed to help relevant departments issue acceptance reports. Choosing the data of 4 wires from one phase for analysis, 1035 frames of image are collected. The imaging times of the X-ray images are shown in Fig. 13a. The average detection time per frame is 5.9s, and the minimum time is 4s. In the test, the robot will be affected by short-term gust, which results in the failure of imaging clarity evaluation. So the re-detection leads to longer detection time of a single frame. In addition, the effective length of each frame d_E is 0.145 m, so the detection speed is 1.47 m/min on average.

After analyzing the detection images, as shown in Fig. 13b, the sharpnesses of 99.8% of the images are higher than 0.8. So the image resolution qualification rate is 99.8%. All the 1035 frames are diagnosed by the intelligent diagnosis system, and 35 suspected defects appear. After the manual diagnosis, all the suspected defects are identified as misdiagnosis cases, which are caused by the outer enveloped-aluminum shadow or some foreign bodies on the wires. The misdiagnosis rate of the defect diagnosis system is 3.3%, and it is better to find suspected defects than to miss defects. The experimental results prove that the proposed robot meets the requirements of practical use.

V. CONCLUSION

In this paper, the design and implementation of LineSpyX, an inspection robot for overhead ACCC wires, is introduced. The robot body is all-metal, wrapped-structured and sideway-installing, ensuring sufficient safety and mechanical strength. The moving system is powerful and adaptive, providing a good motion performance to complete the detection task of damageable parts of the ACCC wires. The optimization of robot moving system is done by theoretical and simulation analysis. The moving capabilities of the proposed robot are verified by lab experiments and field tests. The maximum climbing angle of the robot on the wire without obstacle is 35 degrees and is close to 25 degrees on the wire with a vibration damper.

The NDT system based on DR, along with the deep learning based intelligent defect diagnosis system and the defect marking module, realize the detection and localization of defects in ACCC wires. The average detection time per frame is 5.9s, and the average detection speed is 1.47m/min. The experimental results show that the imaging qualification rate is 99.8%, and the misdiagnosis rate is 3.3%. The proposed robot meets the requirements of practical use.

REFERENCES

[1] O. Menendez, FAA. Cheein, M. Perez, and S. Kouro, "Robotics in power systems: Enabling a more reliable and safe grid," IEEE Industrial Electronics Magazine, vol.11, no.2, pp. 22-34, 2017.

[2] J. Katrasnik, P. Franjo, and L. Bostjan. "A survey of mobile robots for distribution power line inspection," IEEE Transactions on power delivery, vol. 25, no.1, pp. 485-493, 2009.

[3] PL. Richard, N Pouliot, F Morin, M. Lepage, P. Mamelin, and S. Montambault, "LineRanger: Analysis and Field Testing of an Innovative Robot for Efficient Assessment of Bundled High-Voltage Powerlines," in International Conference on Robotics and Automation (ICRA), 2019, pp. 9130-9136.

[4] J. Bian, X. Hui, X. Zhao, and M. Tan. "A novel monocular-based navigation approach for UAV autonomous transmission-line inspection," in IEEE/RSJ International Conference on Intelligent Robots and Systems (IROS), 2018, pp. 1-7.

[5] D. Yang, Z. Feng, X. Ren, and N. Lu. "A novel power line inspection robot with dual-parallelogram architecture and its vibration suppression control," Advanced Robotics, vol. 28, no.12, pp. 807-819, 2014.

[6] A. McFadyen, F. Dayoub, S. Martin, J. Ford, and P. Corke. "Assisted control for semi-autonomous power infrastructure inspection using aerial vehicles." in IEEE/RSJ International Conference on Intelligent Robots and Systems (IROS), 2018, pp. 5719-5726.

[7] W. Chang, G. Yang, J. Yu, Z. Liang, L. Cheng, and C. Zhou. "Development of a power line inspection robot with hybrid operation modes," in IEEE/RSJ International Conference on Intelligent Robots and Systems (IROS), 2017, pp. 973-978.

[8] G. Notomista, Y. Emam, and M. Egerstedt. "The SlothBot: A Novel Design for a Wire-Traversing Robot," IEEE Robotics and Automation Letters, vol.4, no.2, pp. 1993-1998, 2019.

[9] Y. Song, H. Wang, Z. Li, and Y. Jiang, "Vision based transmission line broken strand detection and robot behaviour planning," Jiqiren/Robot, vol.37, no.2, pp. 204-211, 2015.

[10] P. Debenest, M. Guarnieri, K. Takita, EF. Fukushima, S. Hirose, K.Tamura, and Y. Morimura. "Expliner–toward a practical robot for inspection of high-voltage lines," Springer Tracts in Advanced Robotics, vol. 62, pp. 45-55, 2010.

[11] V. Banthia, Y. Maddahi, K. Zareinia, S. Liao, T. Olson, WK. Fung, and N. Sepehri, "A prototype telerobotic platform for live transmission line maintenance: Review of design and development," Transactions of the Institute of Measurement and Control, vol. 40, no. 11, pp. 3273-3292, 2018.

[12] N. Pouliot, and M. Serge, "Geometric design of the LineScout, a teleoperated robot for power line inspection and maintenance," in IEEE International Conference on Robotics and Automation, 2008, pp. 3970-3977.

[13] W. Jiang, Z. Zhou, Y. Yan, G. Wu, L. Yu, H. Li, and W. Chen, "Fuzzy control-based bolt tightening for power cable maintenance robot," Industrial Robot: An International Journal, vol. 45, no.4, pp. 561-571, 2018.

[14] Y. Wang, S. Wei, F. Yin, Y. Yang, L. Tan, and W. Cao, "Review on key technology of de-icing robot running on overhead transmission line," Chinese Journal of Mechanical Engineering, vol.47, no. 23, pp. 30-38, 2011.

[15] A. V. Pinto, M. Z. Sebrao, C. R. S. H. Lourenco, I. S. de Almeida, and J. Saad. "Remote detection of internal corrosion in conductor cables of power transmission lines," International Conference on Applied Robotics for the Power Industry, 2010, pp. 1-6.

[16] X. Jiang, Y. Xia, and J. Hu. (2011). "Optimal design of mfl sensor for detecting broken steel strands in overhead power line," Progress in Electromagnetics Research, vol. 121, pp. 301-311, 2011.

[17] N. Pouliot, E. Lavoie, G. Rousseau, and S. Montambault, "An integrated approach for non-destructive testing of ACSR conductors: Early deployments of robotized sensors," in Proceedings of the 2014 3rd International Conference on Applied Robotics for the Power Industry, 2014, pp. 1-6.

[18] F. Mirallès, P. Hamelin, G. Lambert, S. Lavoie, N. Pouliot, M. Montfrond, and S. Montambault, "LineDrone Technology: Landing an Unmanned Aerial Vehicle on a Power Line," in IEEE International Conference on Robotics and Automation (ICRA), 2018, pp. 6545-6552.

[19] TXR(2018). Self-propelled electric wire inspector [online]. Available: http://www.tsukubatech.co.jp

[20] Yücel, K. Mehmet, M. Legg, V. Kappatos, T. H. Gan. "An ultrasonic guided wave approach for the inspection of overhead transmission line cables," Applied Acoustics, vol.122, pp. 23-34, 2017.

[21] R. J. Hamidi, S. H. Hosseinian, S. H. H. Sadeghi, and Z. Qu. "A Novel Approach to Utilize PLC to Detect Corroded and Eroded Segments of Power Transmission Lines," IEEE Transactions on Power Delivery, vol. 30, no. 2, pp. 746-754, 2015.

[22] F. Lv, P. Zhang, Z. Tang, Y. Yue, and K. Yang. "A guided wave transducer with sprayed magnetostrictive powder coating for monitoring of aluminum conductor steel-reinforced cables," Sensors, vol. 19, no. 7, pp.1-5, 2019.

[23] W. Ji, X. Li, and J. Jia, "Image Recognition and Data Analysis of Ray Detection for Titanium Alloy Pipe Fitting Welding Seam," China Mechanical Engineering, vol.46, no.5, pp.631-641, 2013.

[24] T. Oh, J. Park, K. Seshadrinathan, S. Lee, and AC. Bovik, "No-reference sharpness assessment of camera-shaken images by analysis of spectral structure," IEEE Transactions on Image Processing, vol. 23, no. 12, pp. 5428-5439, 2014.

[25] C. Szegedy, S. Ioffe, V. Vanhoucke, and AA. Alemi, "Inception-v4, inception-resnet and the impact of residual connections on learning," in Thirty-first AAAI conference on artificial intelligence, 2017, pp. 4278-4284